Program Digest, 2019 IEEE International Ultrasonics Symposium (IUS)
Glasgow, Scotland, October 6-9, 2019

Impact Of High Sc Content On Crystal Morphology And RF Performance Of Sputtered $Al_{1-x}Sc_xN$ SMR BAW

Andreas Bogner*†§, Hans-Jörg Timme †, Rüdiger Bauder†, Angelika Mutzbauer†, Diana Pichler†, Michael Krenzer†, Christian Reccius†, Robert Weigel*, Amélie Hagelauer‡

*Institute for Electronics Engineering, University of Erlangen-Nuremberg, 91058 Erlangen, Germany
‡Chair of Communications Electronics, University of Bayreuth, 98447 Bayreuth, Germany
†Infineon Technologies AG, Neubiberg, Germany
§Email: andreas.bogner@fau.de

***Abstract*—Applications using BAW devices benefit from large intrinsic electromechanical coupling materials, e.g. $Al_{1-x}Sc_xN$. This work reports BAW-SMRs using high piezoelectric $Al_{1-x}Sc_xN$ and investigates the relations between Sc content, crystal morphology and resonator RF performance. Finally, key requirements for high quality $Al_{1-x}Sc_xN$ thin-film growth are analyzed and discussed examplary for x = 20at.-%.**

***Keywords*—BAW resonator, BAW-SMR, AlScN, thin-film growth**

I. Introduction

Beside the enhancement of the Q-factor, the increase of the effective electromechanical coupling factor k^2_{eff} of BAW resonators contributes to the latest achievements in acoustic filter design. Both, Q-factor and electromechanical coupling are key requirements in applications where the separation between uplink and downlink of frequency bands is minimal and the respective bandwidth is increased. This applies also to the new radio bands in 5G. Here, filter devices are required to cover bands in the 3.3 to 6 GHz range with rather wide bandwidths [1]. Although BAW resonators can achieve such high frequencies, the BAW technology faces the low intrinsic electromechanical coupling of the commonly used piezoelectric material AlN. Consequently, an increased research in alternative resonators, higher coupling piezoelectric materials and single crystal materials can be observed in recent years [2]–[4].

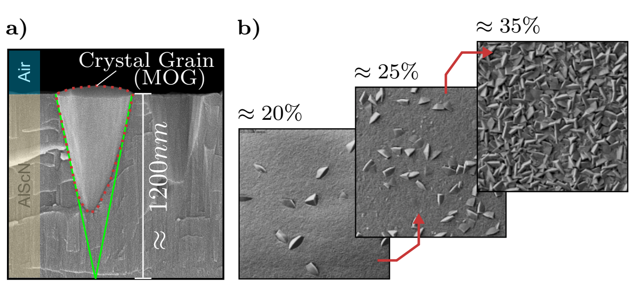

Fig. 1. SEM pictures of the unwanted misoriented crystal grains in $Al_{1-x}Sc_xN$ layers: a) $Al_{0.8}Sc_{0.2}N$ thin-film cross section; b) $Al_{1-x}Sc_xN$ thin-film surfaces for different Sc contents

One of these promising materials is $Al_{1-x}Sc_xN$, which allows to increase the piezoelectric property up to four times by using Sc concentrations up to 43 at.-% [5]. However, the application of BAW resonators comprising AlN with high Sc content is still in its infancy and recent publications report enhanced challenges of thin-film growth for BAW resonators with increasing Sc content. One of these challenges is the occurrence of misoriented crystal grains (see Fig. 1 a)). It decreases the effective electromechanical coupling of BAW devices and impedes further processing [6]. As can be seen in Fig. 1 b), the probability of misoriented crystal grains (MOG) increases with higher Sc content. A theoretical concept of the origin of these MOGs has been given by Sandu et al. [7]. Finally, the material Q-factor seems to be also a problem for high Sc concentrations [1].

This work investigates the challenges of crystal growth and RF performance when using AlN with high Sc content up to 35 at.-%. In addition, the key requirements for high quality thin-film growth are presented and illustrated with SEM and BAW measurement data. For Sc contents of 20 at.-%, it is shown, that the crystal quality and the electrical BAW RF parameters strongly depend on the electrode/$Al_{0.8}Sc_{0.2}N$ interface and can be improved without changing the bulk $Al_{0.8}Sc_{0.2}N$ deposition parameters.

II. Methods

A. Thin-Film Deposition

The 20 at.-% Sc AlN thin-films with a thickness of 1200 nm were grown on different electrodes and seed layers at 350 °C with a pulsed DC magnetron sputtering tool in a 200 mm PVD system. The $Al_{0.8}Sc_{0.2}N$ optimization process was performed using a high-purity AlSc-alloy target (c_{Sc}=18.5 at.-%). Furthermore, the target power, the pulse frequency, the platen RF power as well as the chamber base pressure and magnetron configuration have been kept constant and are similar to standard parameters used for pure AlN deposition. For thin-films with Sc concentra-

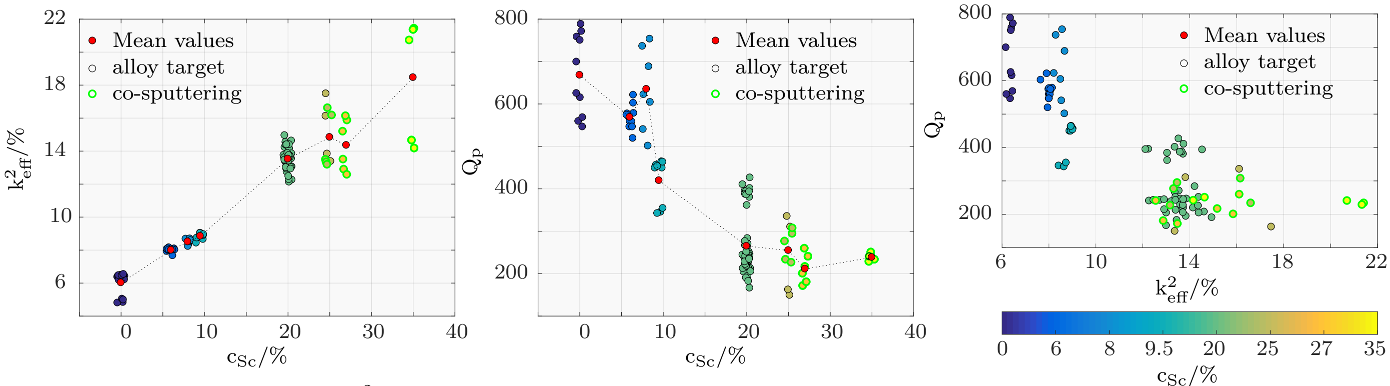

Fig. 2. Overview of Q-factor and k^2_{eff} for various $Al_{1-x}Sc_xN$ growth experiments with different Sc concentrations up to 35at.-% and minor process variations like electrode processing and seed layer variations. Each data point represents a BAW resonator measurement.

tions at 35 at.-%, 27 at.-% and 25 at.-% additionally a co-sputtering method was employed.

B. Structural & Chemical Characterization

For the thin-film characterization scanning electron microscopy (SEM) pictures were taken of all $Al_{1-x}Sc_xN$ thin-films. For a more detailed analysis of the crystal morphology one of the 20 at.-% Sc $Al_{1-x}Sc_xN$ samples was investigated also by scanning transmission electron microscopy (STEM) and X-ray diffraction (XRD). The cross-section specimen for STEM at wafer center and edge are prepared using a FIB (focus ion beam) lift-out technique. The extracted sample is finally thinned to 50 - 100 nm. For a better understanding of the abnormal crystal grains, the elongated sample at wafer center was chosen in a way, that it also contains the cross-section of one of the MOGs. Furthermore, energy dispersive X-ray mapping scans were taken of the STEM lamella to get an estimation of the Sc content.

C. BAW Technology & RF Characterization

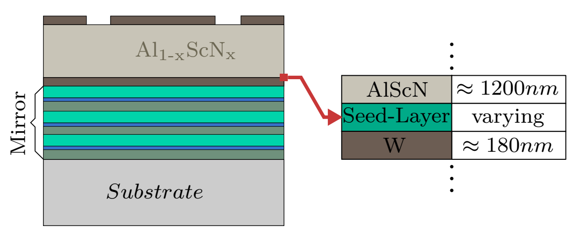

Fig. 3. Schematic illustration of the simplified BAW resonator cross-section with squared electrodes for RF characterization and focus on the critical layers for high quality crystal growth of $Al_{1-x}Sc_xN$

In order to study the material Q-factor, the effective electromechanical coupling factor k^2_{eff} and the relations between thin-film quality and RF performance, a simplified squared resonator of the solidly mounted BAW resonator type was fabricated at 2 GHz for pure AlN. To trap the acoustic energy inside the resonator an alternating SiO2/W mirror was designed to cover longitudinal and shear wave modes. From published material characterization experiments it is known, that the stiffness, the longitudinal and shear velocities decrease with increasing Sc content. Consequently, the mirror transmissivity was optimized to cover also lower resonance frequencies up to 1.4 GHz. For the design process a best guess of the $Al_{1-x}Sc_xN$ material parameters was obtained from literature. Apart from some seed layer variations, all measurements in this work use the same BAW layer stack and layer thicknesses. A schematic drawing of the resonator is given in Fig. 3.

The effective electromechanical coupling coefficient k^2_{eff} of BAW resonators is derived by:

$$k^2_{eff} = \frac{\pi}{2}\frac{f_s}{f_p}\cot\left(\frac{\pi}{2}\frac{f_s}{f_p}\right). \qquad (1)$$

The phase slope of the BAW resonator impedance determines the resonator's Q-factor:

$$Q_{s,p} = \frac{f_{s,p}}{2}\left|\frac{d\phi}{df}\right|_{f=f_s,f_p}. \qquad (2)$$

III. Measurement Results & Discussion

Within this work, $Al_{1-x}Sc_xN$ based BAW resonators of the SMR-type were fabricated for Sc concentrations up to 35at.-%. Their characteristic parameters Q_p and k^2_{eff} were extracted and discussed. Furthermore, the $Al_{0.8}Sc_{0.2}N$ layers were characterized by SEM, STEM and XRD to optimize its crystal morphology and to compare it to the resonator's RF performance.

A. Sc Content vs. RF Performance

Fig. 2 a) to c) show the extracted effective electromechanical coupling values and Q-factors of numerous BAW resonator measurements. Apart from different seed layers and preconditioning steps, all of them are processed with the same layer stack and thicknesses. Furthermore, they differ in the sputtering method (co-sputtering, single alloy target) and the wafer position (center, edge). As expected, k^2_{eff} increases for higher Sc concentrations. The highest obtained value is k^2_{eff}=21 % using a co-sputtering method with 35 at.-% Sc. On the other hand, the Q-factor at parallel resonance is decreasing with ascending Sc concentrations. However, for each Sc concentration a large variation in Q-factor and k_{eff}^2 can be observed. This can be primarily contributed to the different seed layers, preconditioning variations and sputtering configurations, that result in different crystal morphologies of the resulting $Al_{1-x}Sc_xN$ thin-films. Nevertheless, it is highly probable that even without MOGs and reasonable c-axis orientation of the polycrystalline thin-film, the material Q decreases with increasing Sc content. Yet, it is worth mentioning, that the $Al_{1-x}Sc_xN$-BAW resonator performance can be drastically improved by adjusting the initial growth conditions, which can be seen in the next sections.

B. Growth of $Al_{1-x}Sc_xN$ Thin-Films

Exemplary bulk $Al_{0.8}Sc_{0.2}N$ depositions with different seed layers, but otherwise constant process parameters and their respective rocking curve full-width of half-maximum (RC FWHM), k_{eff}^2 and Q_p values are depicted in Fig. 4. The variations in crystal morphology show a high sensitivity of the $Al_{1-x}Sc_xN$ growth to the initial conditions. Only the experiment with 30 nm Ti + 30 nm Pt as seed layer shows measurable results in the wafer center and wafer edge as well. Different to pure AlN thin-films, it seems to be more critical to find a proper growth condition. Actually, choosing the right electrode treatment and/or seed material as well as thickness can be crucial for success when growing $Al_{1-x}Sc_xN$ layers with high Sc content. A recurring phenomenon in the SEM pictures of the thin-film surfaces is the equally sized protruding MOGs (see Fig. 1), which might be due to a common growth start of the MOGs. According to the conceptual elongation of the grain boundaries in SEM/STEM cross section pictures, the MOG growth start is expected to be somewhere at the electrode/$Al_{1-x}Sc_xN$ interface (see green line Fig. 5). Consequently, the setting of the initial growth conditions is seen as one of most critical parameters for MOG-free and high-Q $Al_{1-x}Sc_xN$ thin-films.

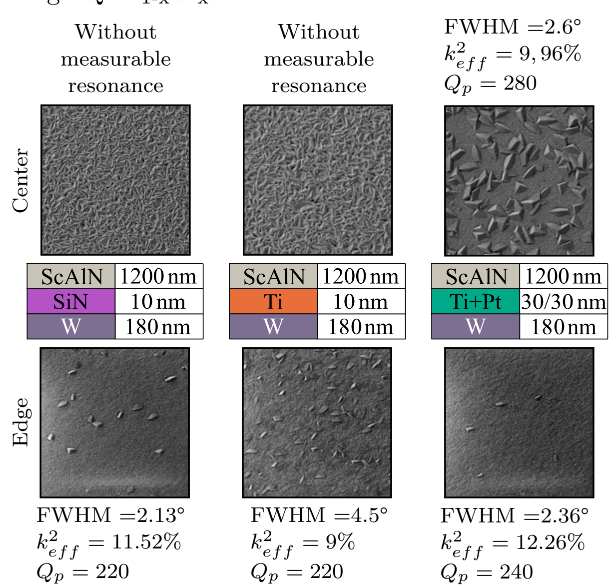

Fig. 4. Exemplary thin-film growth results on different seed layers with SEM pictures and the respective RF parameter Q and k_{eff}^2.

Furthermore, it is expected that another challenging aspect of $Al_{1-x}Sc_xN$ growth is to find a robust process flow, that also allows good thin-film growth at different Sc concentrations.

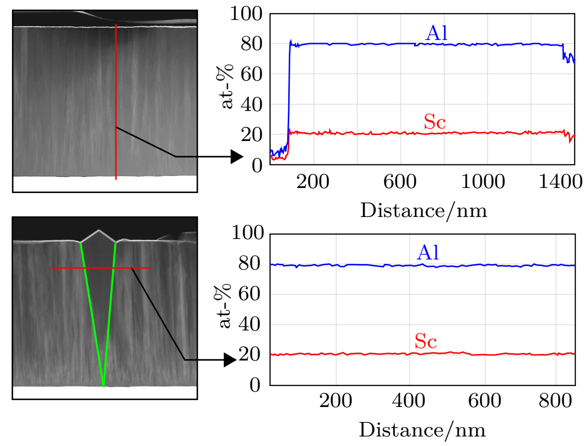

Fig. 5. Scanning transmission electron microscopy results with electron diffraction scanning along red lines for determination of Sc concentrations in the $Al_{0.8}Sc_{0.2}N$ thin-films.

Based on the previously stated assumptions, various seed layer as well as electrode processing steps, like polishing and rinsing are tested in the following section to find suitable starting conditions for the $Al_{0.8}Sc_{0.2}N$ growth.

C. Optimized $Al_{0.8}Sc_{0.2}N$ thin-films

According to the findings the layer optimization is focused on the adjustment of the electrode/$Al_{1-x}Sc_xN$ interface. Therefore, the 18.5at.-% AlSc-alloy target and equal $Al_{1-x}Sc_xN$ deposition parameters for every wafer were employed. According to the EDS mapping, the resulting $Al_{1-x}Sc_xN$ thin-films show around 20 at.-% Sc content (see Fig. 5). The continuous improvement by changing the initial growth conditions through seed layers and electrode treatments is given in Fig. 6. SEM pictures of the wafer center and wafer edge as well as the RF parameters are depicted. Comparing the optical results with the electrical RF parameter shows a clear correlation. Again, it can be seen, that for less MOGs a better coupling can be achieved. However, a small amount of MOGs doesn't seem to have too much of an effect to the effective coupling (see wafer 5 to 7 in Fig. 6). It is worth mentioning that also some process variations in layer thickness can change the actual effective electromechanical coupling. In addition, the Q-factor slightly depends on the occurrence of MOGs. However, this relation has no strong interdependence, as can be seen when comparing the results from experiment 6 and 7. There is hardly any difference in the SEM results, which is also reflected by the effective electromechanical coupling coefficient. Nevertheless, a clear difference in the Q-factors is observable. A reason could be the change in the columnar grain size. The XRD results of the optimized wafer shows a RC FWHM of 1.6°. The final optimized

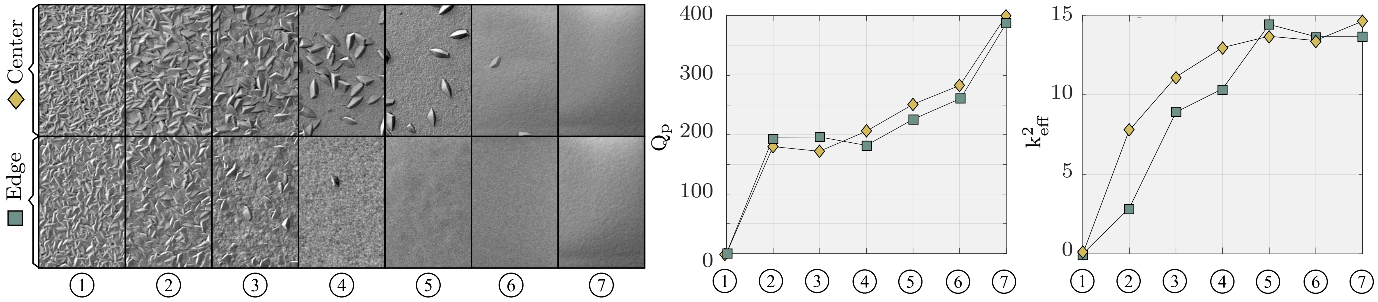

Fig. 6. View of SEM and RF parameter results for continuously improved $Al_{1\text{-}x}Sc_xN$ thin-films by adjustements of the electrode/$Al_{1\text{-}x}Sc_xN$ interface. Each slot (1-7) represents an experiment with varied interface conditions.

process flow of wafer 7 in Fig. 6 shows no MOGs and high effective electromechanical coupling. Regarding the Q-factor, it is important to note that the resonator design is rather simple and no spurious mode suppression was employed. Furthermore, we cannot guarantee that the mirror shows the initially designed characteristics due to process variations and material parameter deviations. Thus, it is expected, that a proper processing and improved resonator design would lead to much higher Q-factors. Nevertheless, the SEM and RF characterization results of the optimized thin-film clearly indicate high crystal quality and process robustness without changing the standard bulk deposition parameters. Finally, a wafer map of the optimized thin-film BAW RF parameters is given in Fig. 7. The best effective electromechanical coupling is observed in wafer center and the resonator Q-factors are distributed with high uniformity, which is an important aspect for high volume mass production.

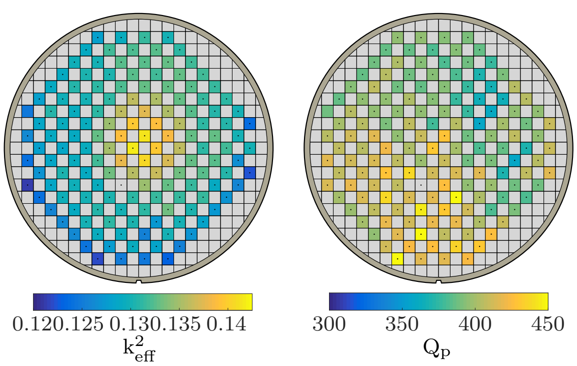

Fig. 7. Wafer map of Q and k^2_{eff} for the optimized $Al_{1\text{-}x}Sc_xN$ thin-film.

IV. Conclusion

The growth and RF performance of $Al_{1\text{-}x}Sc_xN$ thin-films have been studied by structural analysis and simple BAW resonator designs. The crystal morphology of $Al_{1\text{-}x}Sc_xN$ thin-films and respective BAW resonator parameters of the SMR-type were found to vary strongly with seed layer material and electrode surface condition. Improved $Al_{1\text{-}x}Sc_xN$ thin-films were obtained by testing different seed layers and several electrode cleaning, rinsing and polishing experiments. The sputtering of $Al_{1\text{-}x}Sc_xN$ on top of these improved initial conditions allowed the growth of dense columnar grains without any MOGs. We conclude to account for the following criteria for high-Q polycrystalline $Al_{1\text{-}x}Sc_xN$ layers in BAW technology up to 35 at.-% Sc:

1) Top mirror layer (low roughness)
2) Electrode material & deposition (low roughness)
3) Electrode surface treatment (cleaning/rinsing)
4) Seed layer material & deposition
5) Seed layer thickness

The given criteria become even more important with higher frequencies since the deposited layers get thinner and piezoelectric layer properties depend more and more on the layers below. Finally, we found that only by combination of all criteria a high c-axis oriented thin-film is derived.

Acknowledgement

The authors would like to thank W. Breuer and T. Forster for the device measurements and the Infineon Regensburg staff for their support with device fabrication.

References

[1] R. Aigner et al., "BAW filters for 5G bands", IEEE IEDM, 14.5.1-14.5.4, 2018.

[2] V. Plessky et al., "5 GHz laterally-excited bulk-wave resonators (XBARs) based on thin platelets of lithium niobate", Electronics Letters, vol. 55, no. 2, pp. 98–100, 2019.

[3] T. Yokoyama, Y. Iwazaki, T. Nishihara, and J. Tsutsumi, "Dopant concentration dependence of electromechanical coupling coefficients of co-doped AlN thin-films for BAW devices", IEEE IUS, pp. 1–4, 2016.

[4] R. Vetury, M. D. Hodge, and J. B. Shealy, "High power, wideband single crystal XBAW technology for sub-6 GHz micro RF filter applications", IEEE IUS, pp. 206–212, 2018.

[5] M. Akiyama et al., "Enhancement of piezoelectric response in scandium aluminum nitride alloy thin-films prepared by dual reactive cosputtering", Adv. Mater., vol. 21, no. 5, pp. 593–596, 2009.

[6] S. Fichtner et al., "Identifying and overcoming the interface originating c-axis instability in highly Sc enhanced AlN for piezoelectric micro-electromechanical systems", J. Appl. Phys., vol. 122, no. 3, 35301, 2017.

[7] C. S. Sandu et al., "Abnormal grain growth in AlScN thin films induced by complexion formation at crystallite interfaces," Phys. Stat. Sol. A, vol. 95, 1800569, 2018.